SUPPLEMENTAL MATERIAL

Illustrative toy example

In this appendix we illustrate the old method, which assumes a Killing horizon, and the new ingoing method described in this paper, using a simple toy example; numerically finding the Schwarzschild solution assuming spherical symmetry. The purpose is to contrast the two methods, and illustrate explicitly how to use them in as simple a context as possible. We hope this will be of use to a reader interested in actually implementing these methods in more complicated settings.

The old Killing horizon method

We write an ansatz for the black hole metric as,

$$ds^2 = -r^2\left(\kappa^2 f B + r^2 A\right)dt^2 + \frac{4B dr^2}{f^4} + \frac{S}{f^2}d\Omega^2 \qquad (9)$$

where $d\Omega^2$ is the line element on the unit round 2-sphere, A, B, S are smooth (at least C^2) functions of a compact coordinate $r \in [0,1]$ and $f(r) = 1 - r^2$. We require $A = B = S = 1$ at $r = 1$ giving asymptotic flatness. Regularity at the horizon $r = 0$ implies that A, B, S must be smooth functions in r^2, and then κ gives the surface gravity.

We may discretize A, B, S on the interval $[0, 1]$ and then require Neumann boundary conditions at $r = 0$ for these functions. As an example, one might take the reference metric and the initial guess to be the above metric with $A = B = 1 - f/2$ and $S = 1$ (which is not Schwarzschild). On finding a solution, one obtains that odd derivatives at $r = 0$ vanish. However this approach suggests there is a boundary at the horizon, which really there is not. A better way to think is solving the problem in the domain $[-1, 1]$ requiring smooth and *even* solutions so $A(-r) = A(r)$ and similarly for B and S. Using finite difference or pseudo-spectral methods one may choose lattices with even numbers of points that avoid $r = 0$ altogether. Then we have no boundary at the horizon and instead solve the problem on the complete $t = 0$ slice representing the Einstein-Rosen bridge that intersects the bifurcation surface.

The new ingoing non-Killing horizon method

Take an ansatz with ingoing time t,

$$ds^2 = -T dt^2 - \frac{2}{z^2}V dt dz + \frac{1}{z^4}A dz^2 + \frac{S}{z^2}d\Omega^2 \qquad (10)$$

for a compact coordinate $z \in [0, 1]$ with T, V, A, S sufficiently smooth (at least C^2) functions of z. We impose asymptotic flatness as $T = V = S = 1$ and $A = 0$ at $z = 0$. For monotonic S the horizon occurs at $T = 0$ and provided V is non-zero and the functions are smooth in z there then the horizon will be regular. Now $z = 1$ is not regarded as a boundary, and the equations (2) of the main text are imposed there as in the interior of the domain. We must impose one condition to select the Schwarzschild solution we wish to find, ie. to choose a mass. A simple way to fix this is that instead of solving the tt component of (2) in the main text at $z = 1$, we replace it with a Dirichlet condition for T at $z = 1$, so $T|_{z=1} = T_{inner}$ where $T_{inner} < 0$ to ensure the domain pierces the horizon [1]. Consider the smooth metric,

$$\bar{ds}^2 = -(1 - \alpha z)dt^2 - \frac{2}{z^2}dtdz + \frac{1 + z^3/10}{z^2}d\Omega^2 \qquad (11)$$

for constant α – note this is not Schwarzschild. As an example let us take this metric with $\alpha = 1.10$ as the reference metric, and with $\alpha = 1.20$ as the initial guess. The Newton method then converges to a solution with $\partial_z T|_{z=0} = -1.06$. Note that had one tried to find a black hole where the horizon was located at $z > 1$, for example taking an initial guess so that $T_{inner} > 0$ then the method fails. The requirement of a smooth horizon is crucial to impose boundary conditions correctly.

Two important points arise in this example. Firstly experimentally we find that for second order finite difference the method fails, presumably as it doesn't impose smoothness of the functions to a sufficient degree. Certainly for fourth order or above the method works very well, as it does for pseudo-spectral differencing. A second point is that if we had not imposed $T = T_{inner}$ at $z = 1$ but only the equations of motion there we would not obtain a locally unique solution. We emphasise that in this ingoing method the reference metric does *not* determine the moduli (in this case mass) of the solutions found.

Details for inhomogeneous plasma flows and their duals

For a given boundary metric deformation specified by the constants α and β, the solution is determined by the parameters r, z_0 as discussed in the main text. We note that the global scaling $x^a = (t, \rho, y) \to \lambda x^a$ of the boundary together with scaling of the parameters $\alpha \to \alpha$ and $\beta \to \lambda^{-1}\beta$, and the boundary stress tensor components, $(G_4\langle T_{ab}\rangle) \to \lambda^{-3}(G_4\langle T_{ab}\rangle)$ relates solutions due to the conformal invariance of the boundary theory. In practice we choose $z_0 = 1$ and $z_{max} = 1.025$, then vary r to obtain the required ingoing velocity v_0 (or equivalently ingoing value of $\langle T^{t\rho}\rangle/\langle T^{tt} + T^{t\rho}\rangle$) which is scale invariant. In principle we would then use the above scaling to generate a solution with the required ingoing temperature T_0 (or equivalently ingoing value of $G_4\langle T_{tt}\rangle$). However, for reasons that we do not understand (presumably related to the details of the way we fix the moduli of the solution) the value of T_0 is actually the same to better than per-

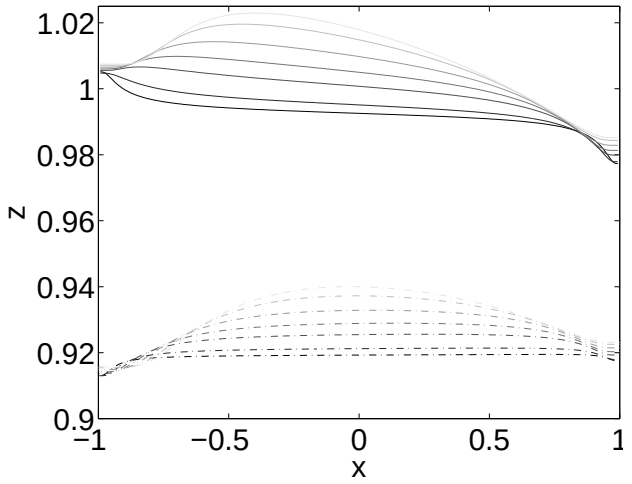

FIG. 3. Coordinate positions of the horizon (solid lines) and ergosurface (dashed lines) for the flows in figure 1 of the main text. The larger the value of β the deeper the horizon penetrates in the z-direction. Entropy is produced along the flow and hence the area density of the horizon is larger on the right end.

cent level for the various values of β we have explored, and so we have not needed to apply any scaling to the data presented here.

In figure 3, we plot the position of the ergoregion (defined by $T = 0$), and the horizon solved from the o.d.e. $g^{\mu\nu}\,\partial_\mu h\,\partial_\nu h = 0$ discussed in the main text. We note that both have a complicated dependence on x, although as expected this vanishes as $x \to \pm 1$ where the metric becomes that of a homogeneous black brane, which in the coordinates defined by our reference metric will have ergoregion and horizon at constant z. Note also that the position of the horizon lies entirely within our domain $0 < z < z_{max} = 1.025$ for all the solutions presented here. Since the metric functions are smooth at the position of the horizon, the future horizon is regular.

We solve the Einstein equations and gauge condition $\xi^\mu = 0$ as a power series in z near the boundary at $z = 0$, and then transforming from our ingoing coordinates to Fefferman-Graham coordinates, we extract the vev of the dual CFT stress tensor from the z^3 terms in the expansions of $T, V, \ldots, A$ using holographic renormalisation [2]. Defining,

$$\frac{16\pi\, G_4}{3}\langle \begin{pmatrix} T_{tt} & T_{\rho t} & 0 \\ T_{\rho t} & T_{\rho\rho} & 0 \\ 0 & 0 & T_{yy} \end{pmatrix}\rangle = \begin{pmatrix} t_3(\rho) & u_3(\rho) & 0 \\ u_3(\rho) & b_3(\rho) & 0 \\ 0 & 0 & s_3(\rho) \end{pmatrix}, \tag{12}$$

then t_3, b_3, u_3, s_3 can be obtained from the bulk solution. For example, for t_3 one finds an equation,

$$\begin{aligned} t_3(x) &= \frac{1}{3} + \frac{1}{3!}\,\partial_z^3 T\big|_{z=0} \\ &- \frac{f^4\big[-4\sigma'(-6+7f) + f(f\sigma^{(3)} - 12x\sigma^{(2)})\big](101 s_r + 5 s_{3r})}{576\sigma} \\ &- \frac{f^5\,\sigma'(-f\,\sigma^{(2)} + 4\,x\,\sigma')(387\,s_r + 47\,s_{3r})}{1024\,\sigma^2} \\ &- \frac{f^6\,(\sigma')^3(5981\,s_r + 993\,s_{3r})}{32768\,\sigma^3}\,, \end{aligned} \tag{13}$$

where we give all functions in terms of the compact coordinate x (rather than ρ), $f(x) = 1 - x^2$ and $s_{kr} = \sinh kr$. However, since the gauge condition $\xi^\mu = 0$ relates the derivatives of the various metric functions, there are 3 other ways to extract t_3 from three z derivatives of the other metric functions than T. For a continuum solution these must all give the same answer, and we use this to test the accuracy of our stress tensor determination shortly. The other b_3, u_3, s_3 can similarly be extracted from three z derivatives of the various metric functions, and again there may be multiple ways to do this which are equivalent on Einstein solutions. The equations of motion also imply that b_3, u_3, s_3 are locally related to t_3 as the stress tensor is traceless and conserved, which again we check shortly.

In figure 4 we display the vev of the T^{tt} component of the holographic stress tensor and compare it with the same component of the viscous hydrodynamic stress tensor, (15), for varying β in analogy with figure 1 in the main text. We see the same agreement with viscous hydrodynamics at small β, with strong deviations from it for $\beta \sim O(1)$. We note that $\langle T^{tt}\rangle$ is well behaved even for the $\beta = 2$ flow which has a superluminal region.

In the figures above we have compared the holographic plasma behaviour extracted from the dual black holes to the viscous hydrodynamics predicted by the fluid/gravity correspondence. This gives a good approximation for $|\beta/T_0| \ll 1$. We now give details about these hydrodynamic fluid flows. Recall that the viscous fluid approximation to the plasma flow from fluid/gravity is determined by the fluid stress tensor[3],

$$\begin{aligned} 16\pi G_4\langle T^{ab}\rangle &= \left(\frac{4}{3}\pi T\right)^3 \left(u^a u^b + \frac{1}{2}P^{ab}\right) \\ &-2\left(\frac{4}{3}\pi T\right)^2 P^{ac}P^{bd}\left(\nabla_{(c}u_{d)} - \frac{1}{2}g^{(b)}_{cd}\nabla^e u_e\right) + O\left(\nabla^2 u\right) \end{aligned} \tag{14}$$

for a 1+2-dimensional boundary metric $ds^2 = g^{(b)}_{ab}dx^a dx^b$, temperature T, 3-velocity u^a with $u^2 = -1$ and with $P_{ab} = u_a u_b + g^{(b)}_{ab}$. The first term is that of an ideal fluid, and the latter is due to shear viscosity. For our flows, we take the 3-velocity in the ρ direction, so $u^a = (\gamma, \gamma v, 0)$, with v the velocity and $\gamma^{-2} = 1 - v^2$. For small but non-vanishing β the viscous term will generate entropy and the fluid deviates from ideal behaviour.

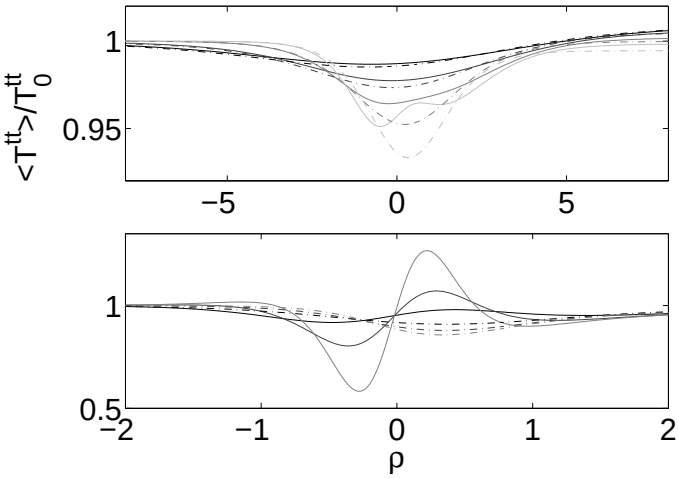

FIG. 4. Plot of $\langle T^{tt}\rangle$ normalised by its ingoing value T_0^{tt} vs. ρ for the holographic stress tensor (solid lines) and the stress tensor of viscous hydrodynamics (dashed lines). *Top*: Flows as in figure 1 of the main text with $\beta = 0.2, 0.3, 0.5, 0.7$. *Bottom*: flows with $\beta = 1., 1.5, 2$. For $\beta \simeq O(1)$ the stress tensor exhibits $O(1)$ features at small scales (compared to the length scale set by the temperature) and hydrodynamics no longer provides a valid description of the flow.

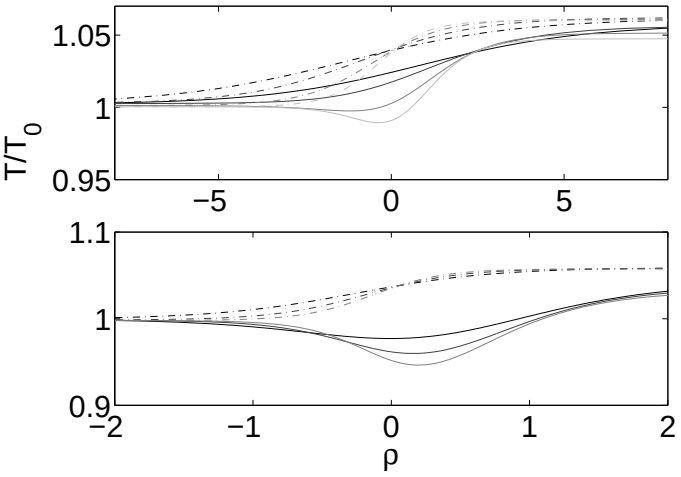

FIG. 5. Temperature, T, plotted normalised by the ingoing temperature T_0 vs. ρ from viscous fluid/gravity hydrodynamics (solid lines) and for ideal fluid/gravity hydrodynamics (dashed lines) used to compare to the holographic plasma flows in figure 1 of the main text and figure 4 here. We emphasise that these only approximate the holographic plasma flow well for small β. *Top:* flows with $\beta = 0.2, 0.3, 0.5, 0.7$. *Bottom:* flows with $\beta = 1., 1.5., 2$. We see for small β agreement between the viscous and ideal hydrodynamics since there is little entropy generation. For larger $\beta \sim O(1)$ viscosity becomes important and the behaviours strongly differ.

The equation of motion for the fluid is given by conservation of this stress tensor. For our boundary metric there are two non-trivial components. One immediately yields $G_4\langle T_{tx}\rangle \propto 1/\sqrt{\sigma}$. Combined with the second, one obtains first order o.d.e.s for the fluid velocity and temperature, as discussed in [4, 5]. It is these we have solved in order to compare to our numerical bulk solutions. In figure 5 we display the behaviour of the temperature for the flows obtained from viscous hydrodynamics which we compared to the stress tensor from the gravity dual in figure 1 of the main text and figure 4 here (we note that the velocity of these hydrodynamic flows are already shown in figure 1 in the main text). For comparison with the viscous hydrodynamics we also show the ideal hydrodynamics solutions for the same ingoing fluid data. We see that as expected, for small β these closely agree, but for $\beta \sim O(1)$ the viscous behaviour departs strongly from the ideal behaviour, and likewise as we have seen in figure 1 of the main text and figure 4 here, deviates from the full plasma behaviour as deduced from the gravity.

Numerical errors and metric functions

For the results presented in this paper we have discretized the harmonic Einstein equation using sixth order finite differencing, taking a uniform grid with N_z lattice points in the z direction, and $N_x = 4N_z$ lattice points in x. We note that especially for the small β solutions where there are sharp gradients in the function σ near the boundaries of the domain it is important to have sufficient resolution in the x direction to obtain accurate results. We have used resolutions up to $N_z \times N_x = 70 \times 280$ points. Typically we begin by finding solutions at lower resolutions, and then use these as initial data to find the higher resolution solutions.

We characterise the numerical error in our solutions by computing the error in solving the Einstein equations as,

$$\begin{aligned}
\mathcal{E}_1 &= \max_{0<z<H(x)} \left| \frac{R}{12} + 1 \right| , \\
\mathcal{E}_2 &= \max_{0<z<H(x)} \left| \frac{R_{\mu\nu}R^{\mu\nu}}{36} - 1 \right| , \\
\mathcal{E}_3 &= \max_{0<z<H(x)} \sqrt{|\xi^\mu \xi_\mu|}
\end{aligned} \tag{15}$$

where each is a scalar quantity which should vanish in the continuum for a solution, and is maximised for the solution in the exterior of the horizon. We maximise only over the region exterior to the horizon to obtain a well defined geometric quantity. We note that similar results are obtained when maximising over the entire domain. Typical results of convergence tests are shown for an intermediate value of $\beta = 1$ in figure 6. For the maximum resolutions used, we see that the maximum local error in the solution is better than 10^{-7}, as stated in the text. In addition, $\mathcal{E}_3 \to 0$ in the continuum limit, which indicates that our solutions are not Ricci solitons. Similar results are obtained for the other values of β (including $\beta = 2$) discussed in this paper.

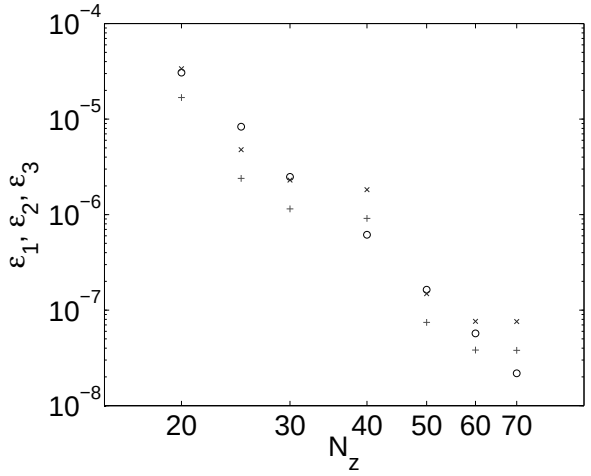

FIG. 6. Convergence plots for the solution with $\beta = 1$. We show $\mathcal{E}_1$ ('o'), $\mathcal{E}_2$ ('x') and $\mathcal{E}_3$ ('+'), which measure the maximum error in the Ricci scalar, Ricci tensor and the magnitude of $\sqrt{|\xi^\mu \xi_\mu|}$ respectively, as a function of the number of grid points in the z-direction, N_z. The resolution in x is given as $N_x = 4N_z$. We see linear convergence in this log-log plot. For $\mathcal{E}_1$ and $\mathcal{E}_2$ we find the slope is ~ 4 indicating fourth order convergence, whilst for $\mathcal{E}_3$ the slope is ~ 6. Other solutions exhibit the same convergence behaviour.

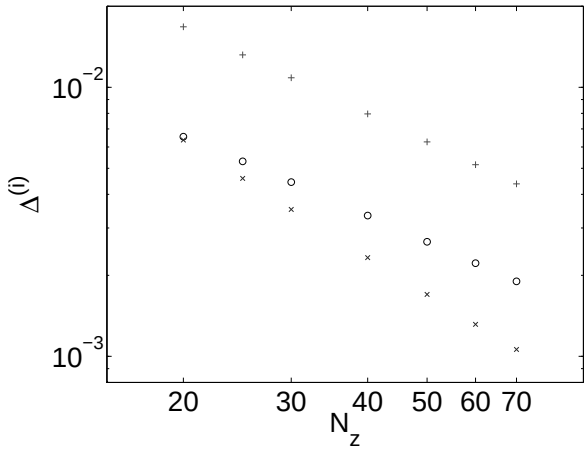

FIG. 7. The function t_3 may be extracted from the metric functions in 4 independent ways which are equivalent in the continuum. Here we plot the maximum value of the three fractional errors, $\Delta^{(i)}$ characterising the deviation between these as a function of the number of grid points in the z direction, N_z, in a log-log scale for the $\beta = 1$ solution. We observe first order (or slightly better) convergence, which is consistent with the overall observed 4^{th} order convergence as the quantity t_3 involves 3 derivatives of the metric functions. We obtain the same results for other values of β.

We note that whilst we have used sixth order finite differencing, the slope of these curves against $\log N_z$ is between $\sim 4-6$ depending on the quantity. We would naively expect ~ 6 for smooth solutions. We believe the observed lack of smoothness is not physical but due to our coordinate choice near the boundaries $x = \pm 1$. Since these boundaries are regular singular points of the p.d.e.s it maybe that there are $(x \mp 1)^p \log|x \mp 1|$ behaviours in the expansions of the metric functions for our gauge choice, where p is some power presumably with $p \geq 4$. We emphasise that we require only second derivatives to be defined for a solution to the Einstein equations, and the convergence we see is certainly much better than that, indicating the metric functions are better than C^2 in smoothness. As we show later, explicit calculation of the various two derivatives of metric functions gives well behaved results, again confirming better than C^2 smoothness. However, the apparent lack of C^∞ smoothness does lead to poor convergence results when using pseudo-spectral differencing, hence our use of finite difference. An obvious future direction is to improve the coordinate choice.

We monitor the errors in the extraction of the stress tensor. As discussed in appendix B the components of the stress tensor $t_3(x)$, $u_3(x)$, $s_3(x)$ and $b_3(x)$ may be extracted from the 7 metric functions in different ways which should agree in the continuum. In figure 7 we display the fractional error in the different ways of extracting t_3:

$$\Delta^{(i)} = \max_{-1<x<1} \left| 1 - \frac{t_3^{(i)}}{t_3^{(0)}} \right| , \quad i = 1, 2, 3 , \tag{16}$$

where $t_3^{(0)}$ denotes the value of t_3 obtained from $\partial_z^3 T|_{z=0}$ as given in equation (13), and $t_3^{(i)}$ correspond to the other values obtained from the remaining independent combinations of metric functions. As this figure shows, $\Delta^{(i)}$ is consistent with vanishing in the continuum limit with a slope ~ 1 in a log-log plot. This is the expected behaviour; from the equations of motion we have seen that we have fourth order convergence and the calculation of t_3 involves taking three derivatives of the metric functions. Therefore we expect the error in this quantity should exhibit approximately first order convergence. We see for our highest resolution data that the maximum fractional error is less than percent level. We obtain analogous results for other components of the stress tensor which may be extracted in multiple ways, which we note includes the test of tracelessness of the stress tensor.

Next we consider the error in the two non-trivial components of the conservation equation of the stress tensor:

$$\begin{aligned} \mathcal{C}_1 &= \max_{-1<x<1} \left| \frac{u_3'}{u_3} + \frac{1}{2}\frac{\sigma'}{\sigma} \right| , \\ \mathcal{C}_2 &= \max_{-1<x<1} \left| \frac{b_3'}{b_3} + \frac{\sigma'}{\sigma}\left(1 + \frac{t_3}{2\, b_3}\right) \right| , \end{aligned} \tag{17}$$

where each quantity should vanish in the continuum limit. In figure 8 we display $\mathcal{C}_1$ and $\mathcal{C}_2$ as a function

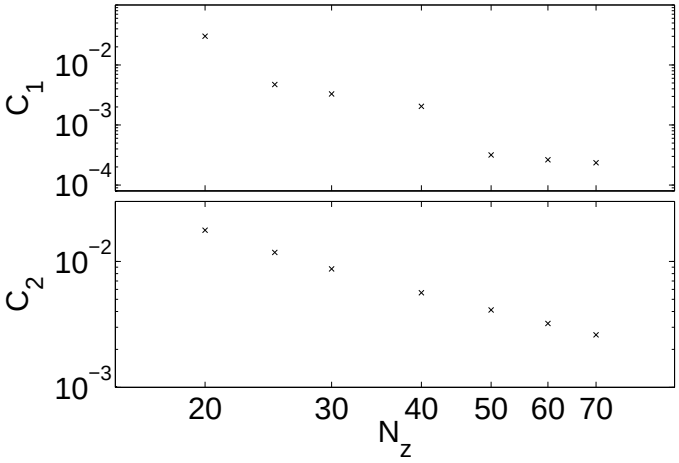

FIG. 8. Convergence plots for $\mathcal{C}_{1,2}$, the maximum errors in the two non-trivial components of the conservation equation for the stress tensor for the $\beta = 1$ solution. The apparent linear convergence in this log-log plot against N_z has slope ~ 4 for $\mathcal{C}_1$, and ~ 1 for C_2. These are consistent (or better) than expected, given the overall 4^{th} order convergence, and that the conservation requires three derivatives of the metric functions in z and one in x.

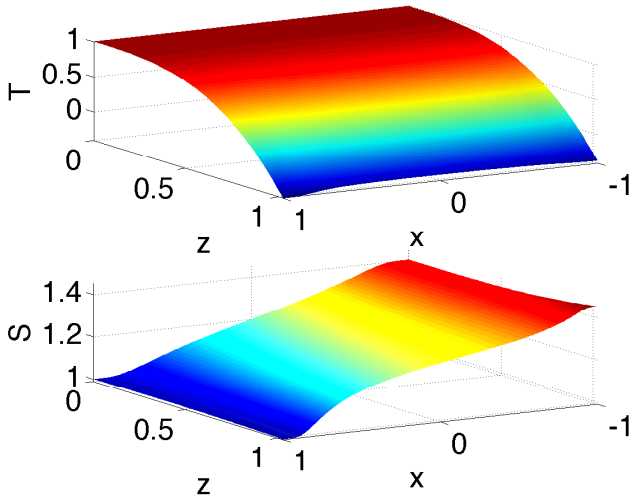

FIG. 9. Metric functions $T(z,x)$ and $S(z,x)$ for the solution with $\beta = 1$. These and the other remaining metric functions V, B, F, U, A, are well behaved everywhere in our domain, including the region inside the horizon.

of the number of grid points in the z direction, N_z, again in a log-log plot. As this figure shows, the error in $\mathcal{C}_1$ exhibits almost fourth order convergence, which is better that one might have naively expected. On the other hand, the convergence in $\mathcal{C}_2$ is slightly better than first order, which is consistent with behaviour of the error in extracting t_3 and b_3 as discussed above. We obtain similar convergence results for the other β studied, including $\beta = 2$.

In summary, our analysis of the numerical errors show that the solutions we present are of high quality, the maximum fractional error in the solutions being better than $\sim 10^{-7}$. The finite differencing method we have implemented gives convergence to the continuum limit consistent with fourth order scaling. Our extraction of the components of the stress tensor exhibits the expected convergence, and we may estimate that the maximum error in these components is better than 1%.

We now turn to the metric functions. For concreteness, in figure 9 we show T and S over the domain for the $\beta = 1$ solution, and note that these are coordinate scalars with respect to z and x coordinate transformations. In figure 10 we show the functions $\partial_x^2 T$ and $\partial_x^2 S$ to illustrate that the metric is better than C^2 and also that derivatives of the metric functions vanish as expected at $x \to \pm 1$ in the coordinate system defined by our reference metric (since the bulk solution becomes a homogeneous black brane there). The other metric functions show the same behaviour as those we show here. Likewise, taking other two derivative combinations of these we obtain analogously well behaved functions. We obtain similarly well behaved metric functions for all other values of β

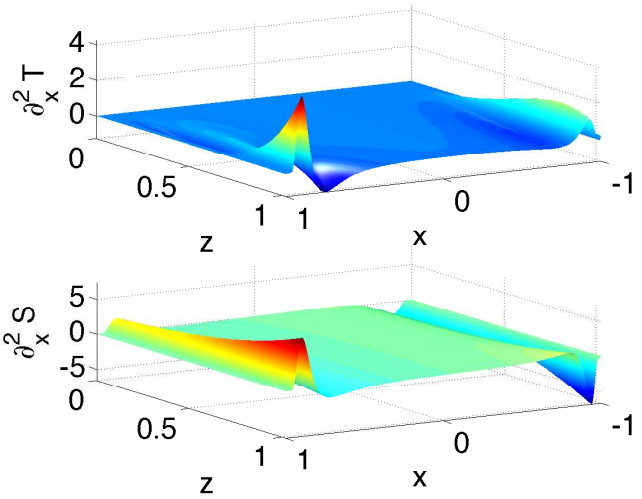

FIG. 10. $\partial_x^2 T$ and $\partial_x^2 S$ for the $\beta = 1$ solution. As expected these are largest where $\sigma(x)$ changes most rapidly. We emphasise that these and other two derivatives of the various metric functions are well behaved over the domain and vanish at the asymptotic ends $x \to \pm 1$ where the flows and dual black brane become homogeneous.

presented here, including $\beta = 2$.

Finally we plot the Weyl curvature as characterised by the scalar $C_{\mu\nu\rho\sigma}C^{\mu\nu\rho\sigma}$ over our domain in figure 11 and note that it is smooth, with no indication of any singular behaviour over the domain, again indicating the metric functions are better than C^2 smooth.

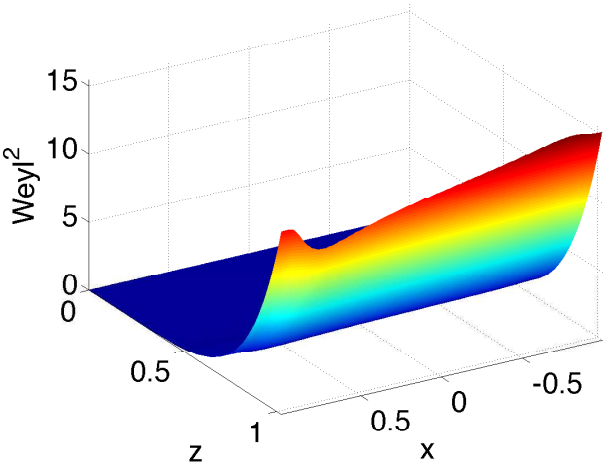

FIG. 11. $C_{\mu\nu\rho\sigma}C^{\mu\nu\rho\sigma}$ for the $\beta = 1$ solution. This function vanishes at the boundary of AdS and well behaved elsewhere, indicating the absence of singularities. At $x \to \pm 1$ where the flow and dual black brane are homogeneous the Weyl tensor also becomes homogeneous, with its x-derivative vanishing.

[1] Instead one can also directly fix the mass m, imposing $\partial_z T|_{z=0} = m$, but we have found this numerically rather unstable in practice.

[2] S. de Haro, S. N. Solodukhin, and K. Skenderis, Commun.Math.Phys. **217**, 595 (2001), arXiv:hep-th/0002230 [hep-th].

[3] S. Bhattacharyya, R. Loganayagam, I. Mandal, S. Minwalla, and A. Sharma, JHEP **0812**, 116 (2008), arXiv:0809.4272 [hep-th].

[4] S. Khlebnikov, M. Kruczenski, and G. Michalogiorgakis, Phys.Rev. **D82**, 125003 (2010), arXiv:1004.3803 [hep-th].

[5] S. Khlebnikov, M. Kruczenski, and G. Michalogiorgakis, JHEP **1107**, 097 (2011), arXiv:1105.1355 [hep-th].